Applied Catalysis B: Environmental 179 (2015) 78–87

Contents lists available at ScienceDirect

Applied Catalysis B: Environmental

journal homepage: www.elsevier.com/locate/apcatb

Comparison of kinetics of acetone, heptane and toluene photocatalytic mineralization over TiO_2 microfibers and Quartzel® mats

M. Le Bechec[a], N. Kinadjian[b], D. Ollis[c], R. Backov[b,1], S. Lacombe[a,*]

[a] IPREM-UMR CNRS 5254, Université de Pau et des Pays de l'Adour, Hélioparc-2 Av. du Président Angot, F-64053 Pau Cedex 09, France
[b] Université de Bordeaux, Centre de Recherche Paul Pascal, Office 115, UPR 8641-CNRS, 115 Avenue Albert Schweitzer, 33600 Pessac, France
[c] Chemical and Biomolelcular Engineering, NCSU, Raleigh, NC 27695, USA

ARTICLE INFO

Article history:
Received 2 February 2015
Received in revised form 29 April 2015
Accepted 6 May 2015
Available online 7 May 2015

Keywords:
Photocatalytic fibers
TiO_2
VOC
Mineralization
Kinetics

ABSTRACT

The kinetic parameters for VOCs (acetone, toluene, heptane) mineralization of lab-extruded pure TiO_2 fibers prepared under easily scalable conditions were compared with those of a commercial photocatalytic media from Saint-Gobain, Quartzel®, under identical conditions. A flow-through recirculating reactor loop with variable LEDs irradiation at 365 nm was specially designed. All the experiments were carried out in a continuous recycle mode. Both types of fibers were very efficient for acetone and heptane mineralization. At 20% relative humidity (RH), the reaction rates were higher with the commercial media, whereas at 60% RH the catalysts displayed equal activity for acetone conversion. Toluene mineralization was much faster on these lab-made fibers than on Quarztel®, which was more sensitive to poisoning by reaction by-products. At 20% relative humidity, with the lab-made TiO_2 fibers, typical quantum efficiencies were, respectively, 0.0106 and 0.0027 for acetone and heptane (100 ppmV initial concentration) and 0.0024 for toluene (200 ppmV initial concentration) while these quantum efficiencies were 0.0358, 0.0133 and 0.0011 with expanded Quartzel fibers under the same conditions. These results evidence a clear difference in the VOCs, water and polar by-products adsorption between these two kinds of fibers.

These newly developed fibers can be produced at an industrial scale with a proven efficiency for VOCs degradation and mineralization. Since they are less sensitive to humidity than the commercial fibers, they could be most useful under actual ambient air conditions. These fibers present a good alternative to other commercially available photocatalytic media for gas phase purification.

1. Introduction

The design of various TiO_2 materials (paints, concretes, cements, mortars, coatings, membranes, textiles and filters) for the oxidation of gaseous pollutants, mainly VOCs and NO_x is currently a topic of interest for decreasing indoor and outdoor air pollution [1–5]. Beyond high crystallinity and large specific surface area required for the degradation of pollutants, TiO_2 may be shaped into various morphologies including nanofibers and nanostructured films or coatings [6–8]. For enhanced specific surface area, 2D (two-dimensional)-mesoporous TiO_2 materials as well as 1D-TiO_2 photocatalyst, such as TiO_2 nanotubes appear as excellent candidates [9–12]. The large surface-to-volume ratio, the enhanced adsorption of various reactants, and the specific morphology of these materials induce a better reactant–catalyst contact while optimizing mass transport, which improves the photocatalytic efficiency.

Among the methods of choice for the fabrication of 1D TiO_2 nanostructures, electrospinning offers several advantages such as simplicity and process control [13–16]. However, some drawbacks inherent to the electrospinning technique have to be overcome. Native fibers are randomly dispersed during the synthesis step, resulting in a direct loss of uni-directionality at the macroscopic scale. Mats of thermally treated random fibers are generally supported on substrates because of their mechanical weakness, limiting the access to their surface area compared to self-standing structures. Lastly, scale-up of electrospinning is still difficult and particular costly for the production of large amounts of materials.

By contrast, conventional wet spinning can be scaled up and is currently used for the industrial production of several synthetic

* Corresponding author. Tel.: +33 559 407 579; fax: +33 559 407 622.
E-mail addresses: ollis@ncsu.edu (D. Ollis), backov@crpp-bordeaux.cnrs.fr (R. Backov), sylvie.lacombe@univ-pau.fr (S. Lacombe).
[1] Tel.: +33 556 845 630; fax: +33 556 845 600.

http://dx.doi.org/10.1016/j.apcatb.2015.05.015
0926-3373/

fibers. This approach based on the injection and coagulation of fiber material dispersed in a liquid was already addressed in our laboratory for the generation of macroscopic carbon nanotube fibers for actuators [17], zinc oxide fibers dedicated to photonics [18], vanadium oxide for gas sensors [19–23] and titania fibers for photocatalysis [24]. The shaping of titania fibers, prepared by extrusion of amorphous titania nanoparticles, latex nanoparticles and non-ionic surfactant in a poly(vinyl) alcohol (PVA) solution containing salts, was gradually improved [25,26] and scaled-up through continuous unidirectional coagulation [18,27] allowing the collection of several tens of meters of TiO_2 fibers. The preparation and characterization of these fibers is extensively described in Supplementary information and detailed in previous papers [24–27]. These fibers had a flattened shape ("tree trunck" with width from 40 to 47 μm and thickness from 10 to 17 μm) and an enhanced bulk macroporosity with large and deep striations at the surface oriented along the fibers main axis. Nitrogen physisorption measurements showed mixed microporous/mesoporous isotherms with specific surface area 110 $m^2 g^{-1}$ and micropore size between 6 and 18 nm. Material roughness was evaluated from the determination of the fractal surface dimension (Ds) deduced from the nitrogen isotherm adsorption curves.[28,29] The Ds value was around 2.55, indicating high surface roughness at the mesoscale. XRD experiments showed that the fibers were mainly anatase, with only minor contribution of brookite phase (10–15%), without any presence of sodium salts remaining after extensive water washing. The crystallites size of the spherical particles calculated from the Debye–Scherrer formula was about 6 nm.

To the best of our knowledge, nanofibers coated with TiO_2 or embedding TiO_2 were only scarcely used for gas-phase pollutants abatement [30,31]. The newly prepared pure TiO_2 microfibers, available at the tens of meters scale, showed an increased efficiency relative to previous thicker ones for acetone degradation in a cylindrical gas phase reactor where the fibers were parallel to the gas flow [25]. Since these thinner microfibers could now be laid out as a soft mat, we intended to more accurately determine their photocatalytic efficiency for volatile organic compounds (VOCs) mineralization in a specially designed flow-through fixed bed reactor with 365 nm LEDs as irradiating source. The mineralization of several VOCs (acetone, heptane and toluene) was studied and carefully compared under identical conditions to a commercial photocatalytic filter, namely Quarztel® from Saint-Gobain composed of quartz fibers coated with TiO_2.

2. Experimental

Two media were tested with the gas-phase setup: a mat of lab-made pure TiO_2 fibers (80 mg) and a commercial Quartzel® medium (Saint Gobain, fiber diameter 9 μm, felt thickness 15–20 mm [32], specific surface area 120 $m^2 g^{-1}$, pore diameters less than 50 nm [33], global density 100 $g m^{-2}$). No additional information is available on this commercial media due to industrial confidentiality. However from the published patents, the titania coating is probably mainly anatase TiO_2 crystallites deposited on the quartz fibers through a sol–gel process [34]. To compare lab-made pure TiO_2 fibers with this commercial media, the same mass of Quartzel® (80 mg) was used and expanded to the same volume (disc of 72 mm diameter and 10 mm thickness). The density of this expanded Quartzel® sample was estimated to 20 $g m^{-2}$ by dividing the mass by the disc volume. To perform the light transmission analysis, we prepared by the same way several expanded samples of Quartzel®: 32 $g m^{-2}$, 66 $g m^{-2}$ and 100 $g m^{-2}$. All these samples were placed between the Pyrex window of the reactor (see below) and the sensor of the spectroradiometer to determine the percent transmission by a given media. During the photocatalytic experiments,

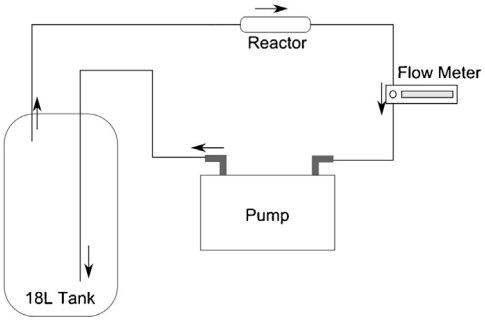

Fig. 1. Simplified scheme of the recirculating loop with a 18 L tank, a Teflon pump, a flow meter and the photocatalytic reactor.

in both cases, at the low face velocity calculated through the media (0.014 $m s^{-1}$), the pressure drop is quite low in these very loose fibers mats (much less than the value for the non-extended original commercial Quartzel® media, which was reported at 30 Pa at 1 $m s^{-1}$). [32]

Photocatalytic mineralization of VOCs was carried out in a batch reactor, based on a PTFE gas-circulating loop where a specifically designed photoreactor was inserted. The loop included a 18 L tank to allow dilution of pollutant, the photocatalytic reactor, a Teflon pump and a flow meter to adjust the flow rate to 3.3 L min^{-1} (Fig. 1). Pressure, temperature and relative humidity (% RH) were recorded during the experiments by sensors connected to the top of the tank. The air was automatically and periodically sampled through a 10 L min^{-1} pump to a Varian 3800 GC equipped with a FID detector (for volatile organic compound (VOC) monitoring) and a methanizer for CO_2 detection.

The photoreactor was designed for the fiber layout as a soft mat (Fig. 2): it was composed of two parts: a cover and a body part. The body is a Pyrex "beaker" with two 1/2 inch Swagelok connections located above and below the catalyst and supporting porous glass disc. The gas had thus to flow through the media. The cover was composed of a Pyrex window inserted in a Teflon part with a Viton O-ring; it could be tightly applied on the body of the reactor and by this way set the reaction volume over the sample (1 cm high, 7.2 cm diameter).

A dedicated LED device was also constructed for this setup: it was composed with 4 high power LEDs (H2A1-H365-E 350 mA Roithner Lasertechnik) giving UVA radiation with a maximum emission at 365 nm (emission spectrum in Fig. S1, Supplementary information), fixed on an aluminum sink to allow heat dispersion. A cooling fan was added on the top of the setup to stabilize the LED temperature and thus the light emission rate. The current intensity can be adjusted between 75 and 350 mA with a homemade LED driver. This LED device can be set inside the Teflon cover very close to the sample (Fig. 2C).

Irradiance measurements were performed with a calibrated spectroradiometer Avaspec 2048L (Avantes) connected to a cosinus corrector (3.9 mm diameter) with an optic fiber (600 μm core diameter). The sensor was placed at 1 cm distance below the Pyrex window at the same position as the photocatalytic media. To map the irradiance on the whole surface of the window, the area was divided by 6×6 squares of 1 cm and the sensor was then placed at every position. The measured light intensity varied from 1 to 9 mW cm^{-2} along the two axes with an intense area at the center (Fig. 3A). Several measurements at different power inputs gave the same distribution of light (data not shown). The influence of the current intensity (88–350 mA) on the irradiance was measured at one central position (Fig. 3B). To determine the light transmission by the photocatalytic media (Fig. 3C and D), the mapping between positions B2 and E5 was recorded without and with media between

the Pyrex window and the sensor at the maximum power input (350 mA). The results of light transmission were expressed as percent of light recorded with media at one position divided by the light recorded at the same position without any media. The average of these 16 values was determined for each media (Fig. 3E).

For all the photocatalytic experiments, the same procedure was followed: once the reactor containing the photocatalytic media was settled in the device, synthetic zero-air was introduced and the relative humidity (RH) was adjusted to the desired value by injecting the required amount of water through a septum on top of the tank or by bubbling air in distilled water. The temperature of the circulating gas was $22 \pm 2\,^{\circ}C$. The samples were first irradiated for 20 h without added VOC under these conditions in order to activate them and analyze the possible evolution of adsorbed VOCs or CO_2 (emission control test). No VOC peak appeared in the chromatograph during this step, but a slow CO_2 increase was noticed due to the leaks of the device and possibly to the photocatalytic degradation of residual organic compounds. The lamps were then switched off. Then the reactor was flushed with fresh zero-air adjusted to suitable RH as previously and 50, 100, 200 or 500 ppmV acetone (respectively, 2.6, 5.2, 10.4 and 26 μL) or 100 ppmV toluene (13 μL) or 200 ppmV heptane (12 μL) was injected in the tank through the septum. After 10 min of equilibration, the lamps were switched on (time 0). VOC and CO_2 concentration was monitored every 7 or 14 min by automatic sampling on the GC-FID and GC-FID-methanizer. In separate dark experiments, the device leaks were determined by monitoring the CO_2 concentration for 20 h (equilibration with outside CO_2) and by monitoring the acetone concentration for 20 h once it has been introduced into the system. The rates of CO_2 entrance from outside atmosphere and of acetone decrease were 0.15 and 0.02 ppmV min^{-1}, respectively (for initial 50 ppmV acetone). The former value was taken into account in the following discussion. An external calibration was regularly checked for conversion of VOCs and CO_2 chromatographic peak area to ppmV.

3. Results

3.1. Light transmission through the photocatalytic mats

With the lab-made LEDs device, the radiant flux measurements made throughout the surface of the reactor showed an intense but inhomogeneous radiant flux with a 4 cm^2 zone of maximum intensity in the center of the reactor whatever the power input (Fig. 3A). Fig. 3B shows that the radiant flux was proportional to the power input. In order to compare both lab-made and commercial media under identical conditions, we decreased the density of the Quartzel® mat by roughly expanding known amounts (previously weighed) of the Quartzel® commercial filter to the same volume (72 mm diameter, 10 mm height). By varying the Quartzel® mat density and by measuring the average radiant flux at different positions of the surface through the reactor containing the photocatalytic media, the light transmission could be determined and compared to the light transmission of the lab-made fibers (Fig. 3E). When the Quartzel® filter was used as received (100 g m^{-2}), only 8.8% light was transmitted. As expected the % transmission decreased with increased Quartzel® mat density and roughly followed an exponential correlation, in agreement with the Beer–Lambert law (Eq. (1)), neglecting scattering by the fibers:

$$\%T = e^{-\epsilon c l} \quad (1)$$

with the optical density $OD = \epsilon c l$, c the TiO_2 density (g cm^{-3}), l the optical path (cm) and ϵ the known absorbance coefficient of TiO_2 at 365 nm (between 1500 and 2500 cm^2 g^{-1}) [35,36]. It was difficult to relate the OD of the Quartzel fibers to the optical path since the % TiO_2 coating (and hence the TiO_2 concentration) on the

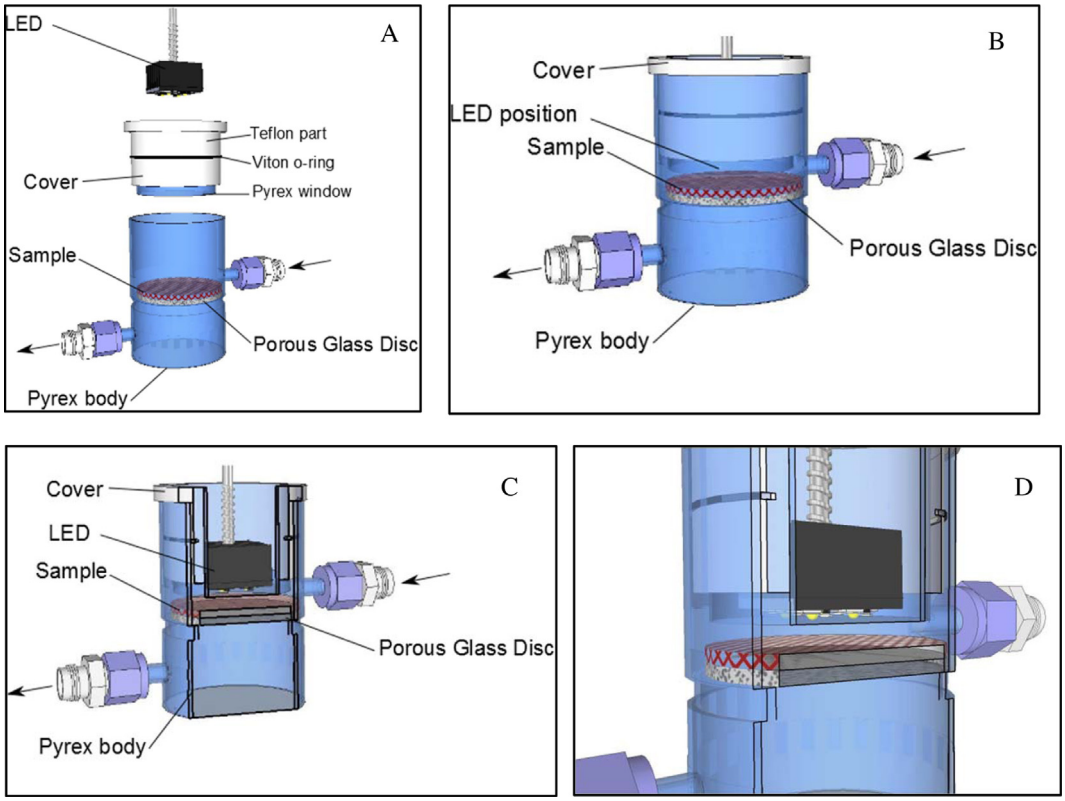

Fig. 2. Schemes of the "Flow Through Photoreactor". (A) Several parts of the reactor: body, cover and lamp. (B) View of the whole reactor. (C and D) Cut views of the mounted reactor.

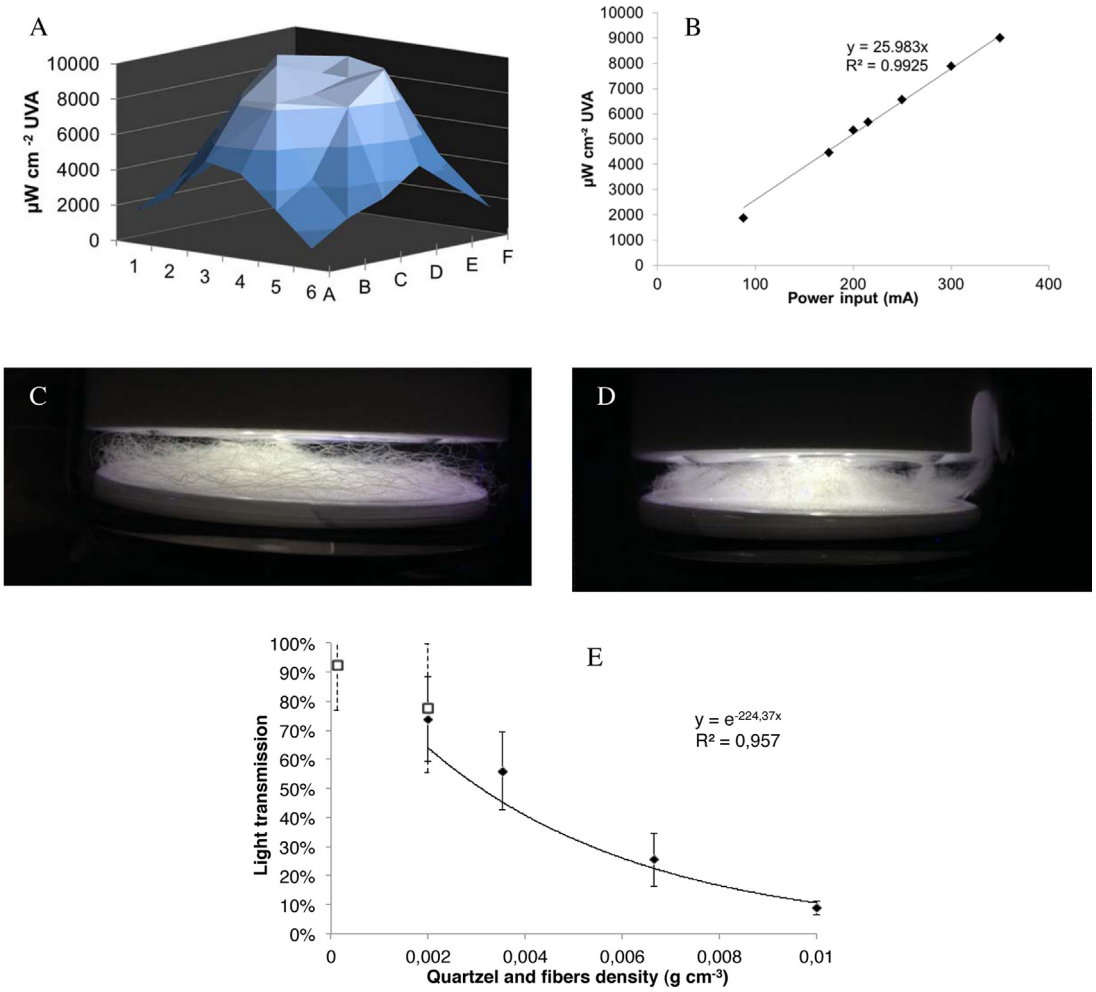

Fig. 3. (A) Mapping of the radiant flux from the LED at the surface of the Pyrex window; (B) correlation between the LEDs current intensity and the radiant flux; (C) picture of the lab-made pure TiO_2 microfibers in the reactor; (D) picture of expanded Quartzel® fibers in the reactor; (E) light transmission through different densities of fiber samples (full diamonds: expanded Quartzel, open square: pure TiO_2 microfibers).

quartz fibers was not provided by the supplier. However, Fig. 3E indicated that light transmission of the lab-made pure TiO_2 fibers correlated quite well with the data of the Quartzel fibers. Taking into account the known quartz density (2.65 g cm^{-3}), the TiO_2 absorbance coefficient, and the density of the material in the reactor, a rough calculation gave about 8% mass of TiO_2 coated on the commercial Quartzel fibers. A parallel calculation on the lab-made fibers, assuming that all the fibers in the reactor volume received the same incident light at this high transmission level (77 %) and taking 3.84 g cm^{-3} as the dense TiO_2 density (neglecting the porosity of the fibers) gave a light penetration in the fibers of about 265 nm. This value was consistent with literature data, generally in the μm or sub-μm range [37–40] and meant that only a small depth of the TiO_2 fiber (width from 40 to 47 μm and thickness from 10 to 17 μm) was absorbing 365 nm irradiation and that the deeper part was not contributing to the photocatalytic reactions. In any case, with the same density (20 g m^{-2}), the lab-made TiO_2 microfibers and the most expanded Quartzel® filter displayed exactly the same average light transmission at 365 nm, ensuring that both media will absorb the same amount of light.

The following comparisons were then carried out with this expanded (20 g m^{-2}) Quartzel media. With this device and with the low amount of media used (80 mg), no dark absorption of any VOC could be observed with either photocatalytic mats: the concentration of introduced VOCs was similar with or without the photocatalytic media. All experiments were thus carried out by switching on the light 10 min after VOC introduction. The following results were obtained with the same sample of fibers (lab-made or Quartzel), only flushing the reactor with fresh humid air after each irradiation.

3.2. Photocatalytic experiments with acetone

Acetone has been extensively used for analyzing gas-phase efficiency of various photocatalytic media due to its easy mineralization without formation of gaseous intermediates [41–45]. The first photocatalytic experiments were carried out with acetone in order to compare the main reaction parameters with both types of media (20 g m^{-2}) under identical conditions (20% RH, 9 mW cm^{-2} at the central point of the reactor).

With both media, a fast decrease of acetone and a fast increase of CO_2 concentrations were observed whatever the initial acetone concentration (Fig. 4A and B for pure TiO_2 microfibers and Fig. 4C and D for expanded Quartzel® filter). In both cases, efficient mineralization to CO_2 was observed, considering that one molecule of acetone should give three molecules of CO_2. Fig. 4A–D show that almost total mineralization was achieved with the lab-made and Quartzel® fibers. At each concentration, the initial rates of acetone degradation (r_A, ppmV min^{-1}) and of CO_2 formation (r_{CO2}, ppmV min^{-1}) were deduced from the initial part of the experimental curves during time $t_{1/2}$ (time to obtain half of the initially introduced acetone concentration). The corresponding values are

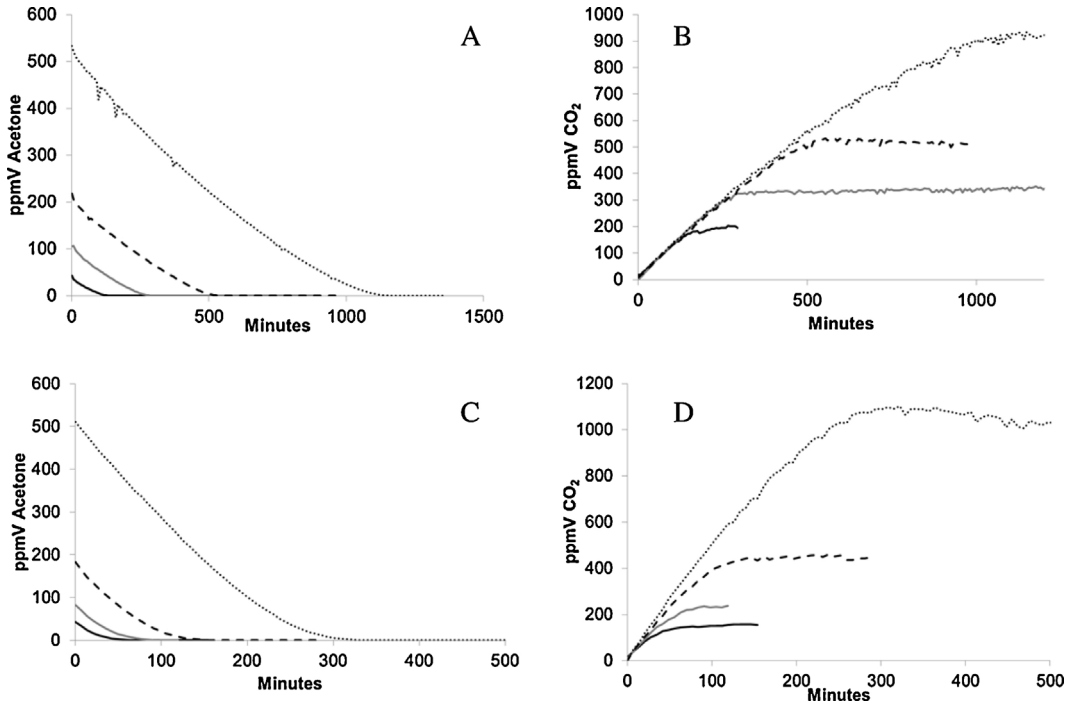

Fig. 4. (A) Acetone concentration against time and (B) CO_2 concentration against time with the irradiated pure TiO_2 microfibers; (C) acetone concentration against time and (D) CO_2 concentration against time with the expanded Quartzel® fibers. (black line 50 ppmV acetone, grey line 100 ppmV acetone, dashed line 200 ppmV acetone and dotted line 500 ppmV acetone); (20% RH, 9 mW cm^{-2} at the central point of the reactor).

gathered Tables T1 and T2 (Supplementary information) and illustrated Fig. 5A and B. From the initial rates of acetone consumption and CO_2 production and from the integrated quantum flux, the quantum efficiency of the catalysts (*i.e.*, the number of moles of acetone degraded ($\Phi_{acetone}$) or of CO_2 formed (Φ_{CO2}) divided by the number of emitted photons) could be calculated (Tables T2 and T3, Fig. S6, Supplementary information). The ratio of these

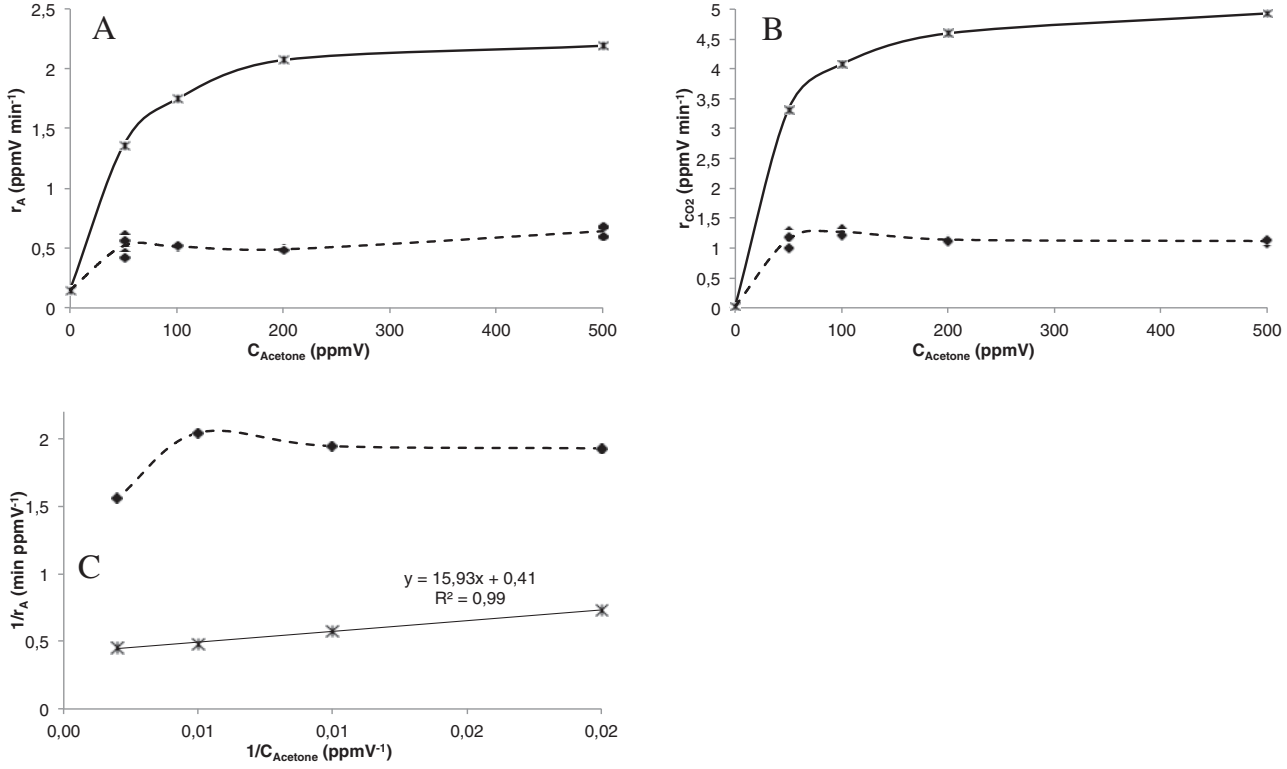

Fig. 5. (A) Initial rate of acetone degradation (r_A); (B) initial rate of CO_2 formation (r_{CO2} *vs* acetone initial concentration C) inverse of initial rate of acetone degradation *vs.* inverse of acetone concentration with pure TiO_2 microfibers (full diamonds, dotted line) and with expanded Quartzel® fibers (*, full line) (20 g m^{-2} in both cases) (20% RH, 9 mW cm^{-2} at the central point of the reactor).

two values gives an estimate of the mineralization yield during time $t_{1/2}$.

3.3. Reaction rate form

According to a previous acetone oxidation study by Ollis [43] and Maudhuit [33] in a similar recirculating loop (containing a monolith coated with 13.8 g of TiO_2 as photocatalytic media in the former case and 3.75 g or 400 cm^2 of Quartzel® media in the latter one), the acetone degradation rate r_A followed a simple Langmuir–Hinshelwood rate form (Eq. (2))

$$r_A = -\frac{kKC}{1+KC} \quad (2)$$

with k the acetone L–H reaction rate constant, K the absorption equilibrium constant, C the acetone gas phase concentration and r_A the acetone reaction rate, taking care of using initial values of C and r_A to avoid any interference with possible by-products. A linear plot of $r_A{}^{-1}$ versus C^{-1} is often obtained that gives the Langmuir absorption equilibrium constant K and k the L–H rate constant.

Plots of reaction rate *vs.* initial concentration showed contrasting behaviors for the two photocatalysts. The Quartzel® data showed a strong variation of rate with concentration (Fig. 5A), and a plot of inverse rate *vs.* inverse concentration was linear (Fig. 5C), demonstrating a good fit to a Langmuir–Hinshelwood inverted rate form (Eq. (3)):

$$\frac{1}{r_A} = \frac{1}{kK}\frac{1}{C} + \frac{1}{k}$$

The reciprocal plot intercept gave $k = 1/0.41 = 2.44$ ppmV min^{-1} and from the slope, $K = 1/(k \times \text{slope}) = 0.026$ $ppmV^{-1}$. The latter value compares well with prior results for photocatalyzed oxidative destruction of acetone over P25 powder ($K = 0.0179$ $ppmV^{-1}$) [42] and P25 coated ceramic monoliths ($K = 0.0297$ $ppmV^{-1}$) [43]. The similar K values for Quartzel® and P25 suggest a similar mixed composition for Quartzel®, even if due to industrial confidentiality, the exact composition of Quartzel® fibers cannot be disclosed, mainly its TiO_2 crystal structure (although probably close to that of Evonik P25 [34,46]).

In contrast to the Quartzel® results, the TiO_2 microfiber catalyst showed nearly a zero order dependence of rate on initial concentration (Fig. 5A and C). We note that our TiO_2 microfibers consist of anatase (85–90%) with a minor component of brookite (10–15 %), whereas P25 is an anatase/rutile mixture. At low (50 ppmV) and high (500 ppmV) acetone concentration, the Quartzel® catalyst was about 3 and 4 times, respectively, as active as our microfibers at 20% relative humidity (Fig. 5A), but was equally active at about 60% RH (see later).

The carbon dioxide generation rates (Fig. 5B) reflected exactly the same kinetic form as found for the reactant rates, namely a Langmuir–Hinshelwood form for Quartzel and a zero order form for the TiO_2 microfiber catalyst.

3.4. Leaks

Atmospheric air contains 0.03% CO_2, thus 300 ppmV CO_2. Any adventitious apparatus leaks could therefore add CO_2 to the overall reactor inventory whenever the reactor CO_2 level was less than 300 ppmV. Above this concentration, the CO_2 leaks would be from the inside to the outside of the reactor, which means that the amount of CO_2 produced would now be underestimated. See for instance the slight downward trend in CO_2 data *vs.* time for 200 ppmV acetone on microfibers and 500 ppmV acetone for Quartzel® in Fig. 4B and D. Accordingly in the following, the calculated errors due to CO_2 leaks are maxima values at CO_2 concentrations >300 ppmV.

The CO_2 generation rate found in the dark represented leaks and/or desorption of adsorbed CO_2 due to heating by the LED sources. The initial formation rates of "dark" CO_2 were 0.144 and 0.173 ppmV min^{-1} for the Quartzel® and TiO_2 microfibers, respectively (Tables T1 and T2, Supplementary information). With the lab-made TiO_2 fibers, at 100 min of irradiation with acetone, the amount of produced CO_2 was always 113 ppmV (Fig. 4B) and leaks could thus account for 15% of total CO_2. With the commercial fibers, at 100 min, the amount of produced CO_2 was in the range 150–500 ppmV (Fig. 4D) and leaks could account for 10 to 3% of total CO_2. At the highest concentration (500 ppmV), 1100 and 300 min were required for total acetone degradation for the Quartzel® and lab-made fibers respectively, and leaks accordingly accounted at maximum for 4 and 20% of total CO_2.

Additional CO_2 could come from desorption of weakly adsorbed CO_2 when the photocatalyst fibers were illuminated, and/or oxidation of residual carbon. However, the initial 20 h illumination treatment for all catalysts should have fully oxidized any carbonaceous contamination.

3.5. Carbon balances

Carbon balances may reveal reaction pathways, as well as the initial presence of carbonaceous species (*e.g.*, adsorbed organic residues) and air leaks.

Total oxidation of acetone will produce 3 mols CO_2 per mol acetone converted. However, the ratio of measured initial reaction rates was only 2.31 mols CO_2 produced per mol acetone converted for the Quartzel® catalyst. Similarly, the TiO_2 microfiber catalyst showed an average of 2.35 mols CO_2 per mol acetone converted at the three lowest concentrations with a significant drop to 1.75 at 500 ppmV acetone concentration (probably due to CO_2 underestimation at these high CO_2 concentrations, see above). The reaction pathway including formaldehyde as a volatile intermediate, as shown below, may rationalize these initial CO_2 generation rates:

$$CH_3COCH_3 \rightarrow CH_2O + 2CO_2(\text{earlytime})$$

$$CH_2O \rightarrow CO_2(\text{latertime})$$

This pathway predicts that early time data would yield two CO_2 molecules per acetone converted, as observed here over both Quartzel® and TiO_2 microfibers.

In a similar vein, Sauer and Ollis [43] earlier explored conversion of acetaldehyde to CO_2, finding release of a single volatile species, formaldehyde (CH_2O), which subsequently mineralized. Thus their apparent pathway was

$$CH_3CHO \rightarrow CH_2O + CO_2(\text{early})$$

$$CH_2O \rightarrow CO_2(\text{later})$$

which would have provided initial ratios of CO_2 generation rates to acetaldehyde conversion rate of unity, lower than the expected eventual stoichiometric ratio of 2.

3.6. Total CO_2

A total carbon balance compares the final CO_2 level measured against the CO_2 expected from total mineralization of the initial acetone. From the data of Fig. 4A–D, we calculated the expected final CO_2 level and the actual CO_2 level measured (Table 1). The errors were estimated by multiplying the rate of CO_2 leaks by the required time for total acetone degradation in each case (overestimated error values at CO_2 concentrations >300 ppmV). For

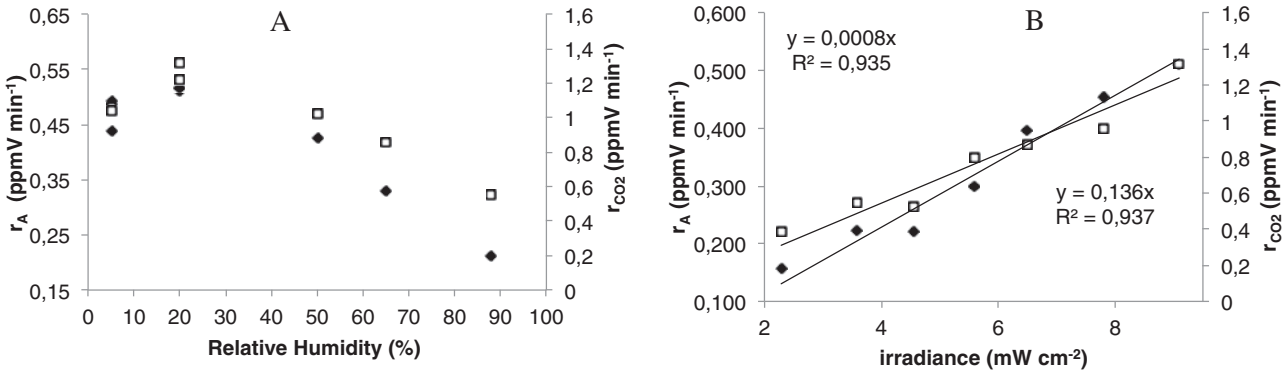

Fig. 6. Initial rate of acetone degradation (r_A, full diamonds) and initial rate of CO_2 formation (r_{CO2}, empty squares) with pure TiO_2 microfibers; (A) at different % RH at 9 mW cm^{-2} at the central point of the reactor; (B) at different irradiance at 20% RH (starting with 100 ppmV acetone in all cases).

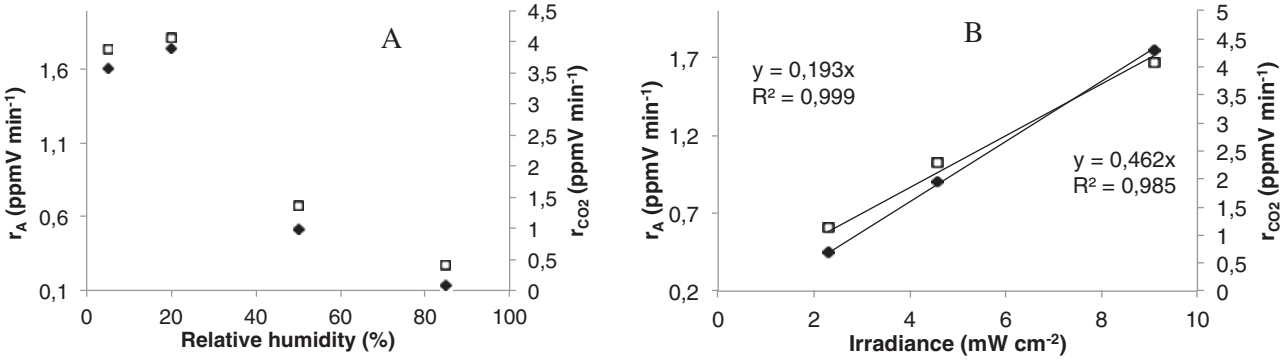

Fig. 7. Initial rate of acetone degradation (r_A, full diamonds) and initial rate of CO_2 formation (r_{CO2}, empty squares) with expanded Quartzel® fibers; (A) at different % RH at 9 mW cm^{-2} at the central point of the reactor; (B) at different irradiance at 20% RH (starting with 100 ppmV acetone in all cases).

Table 1
Expected and actual concentration of carbon dioxide produced upon total acetone degradation on irradiated lab-made TiO_2 and Quartzel® fibers. Data taken from Fig. 4A–D (and Tables T2 and T3, Supplementary information). See text.

Initial acetone	Carbon dioxide (ppmV)				
(ppmV)		Pure TiO_2 microfibers		Quartzel® fibers	
Nominal	Expected	Actual	Extra	Actual	Extra
50	150	202 ± 17	+52	150 ± 7	0
100	300	330 ± 35	+30	230 ± 12	−70
200	600	530 ± 87	−70	440 ± 17	−160
500	1500	1100 ± 190	−400	1100 ± 43	−400

the microfibers, these calculations showed that the observed values were less than the expected CO_2 level at 200–500 ppmV, but almost balanced at the lowest 50 and 100 ppmV initial concentrations. With Quartzel®, the carbon balance was worse in the 100–500 ppmV range, even taking into account the error due to possible leaks, showing a final CO_2 level which is more or less double the initial acetone loading except at the lowest 50 ppmV concentration for which expected and actual CO_2 concentrations are similar.

3.7. Relative humidity and irradiance influence

Further experiments were carried out starting with 100 ppmV acetone and varying either the relative humidity at maximum irradiance (9 mW cm^{-2}) or varying the irradiance at 20% RH. The corresponding rates are gathered in Table T2 (Supplementary information) and in Fig. 6A and B for the pure TiO_2 fibers. Both r_A and r_{CO2} increased to a maximum between 0 and 20% RH, and then decreased by a factor 2.4 (acetone and CO_2) when increasing RH (Fig. 6A). Both rates linearly increased with the radiant flux (Fig. 6B).

With the expanded Quartzel® fibers (Fig. 7A and B), the influence of RH and radiant flux followed the same trends as the microfibers but with a higher sensitivity to % RH since from 20 to 85 % RH, the both rates decreased by a factor 10–13. The slope of the initial rates of CO_2 formation *vs.* radiant flux (Fig. 7B) was also steeper (0.462 min^{-1} mW^{-1} cm^2) with Quartzel® than with the microfibers (0.136 min^{-1} mW^{-1} cm^2). We noted that while Quartzel® is more active at 20% relative humidity, the two catalysts provide equal rates at about 60% RH (Figs. 6 and 7A).

For the lab-made microfibers and Quartzel respectively, the mean calculated quantum efficiency for acetone degradation $\Phi_{acetone}$ (100 ppmV initial concentration, 20% RH) was 1.1 10^{-2} and 3.6 10^{-2}, while the quantum efficiency for CO_2 production Φ_{CO_2} was 2.5×10^{-2} and 8.9×10^{-2} (Table 2). The much stronger influence of relative humidity on Quartzel fibers was also obvious on the quantum efficiency (Tables T2 and T3, Fig. S6, Supplementary information).

3.8. Heptane and toluene

The next experiments were devoted to the compared heptane and toluene mineralization under 20% RH and with the maximum radiant flux (Fig. 8). With both media heptane was efficiently mineralized since starting from 100 ppmV heptane, almost 700 ppmv CO_2 was obtained, as expected from stoichiometry. The rates at 20% RH (Tables T2 and T3, Supplementary information) were still 4 to 5 times higher with Quartzel® (0.659 for heptane and 4.061 ppmV min^{-1} for CO_2) than for the pure TiO_2 microfibers (0.133 min^{-1} for heptane and 0.908 ppmV min^{-1} for CO_2). Similarly, the quantum efficiency for heptane degradation

Table 2
Calculated quantum efficiency of VOC degradation Φ_{VOC} and of CO_2 production Φ_{CO2} under the following conditions: 100 ppmV initial VOC concentration except toluene (200 ppmV), 20% RH. All data are available in Supplementary information, Tables T2 and T3, Fig. S6.

Pollutant	Lab-made pure TiO_2 microfibers			Quartzel® fibers		
	Φ_{VOC} (10^{-2})	Φ_{CO2} (10^{-2})	Ratio Φ_{CO2}/Φ_{VOC}	Φ_{VOC} (10^{-2})	Φ_{CO2} (10^{-2})	Ratio Φ_{CO2}/Φ_{VOC}
Acetone	1.03	2.56	2.5	3.51	8.19	2.3
Heptane	0.27	1.83	6.8	1.33	8.19	6.2
Toluene[a]	0.24	0.93	3.9	0.10	0.28	2.6

[a] Second lower step of the reaction. See text.

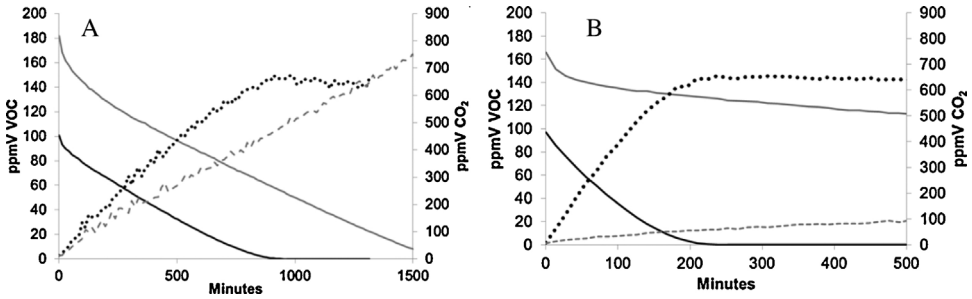

Fig. 8. Concentration of heptane (C_0 100 ppmV, black line), toluene (C_0 200 ppmV, grey line) and CO_2 against time (dark dots with heptane and grey dashes with Toluene) with (A) pure TiO_2 microfibers; (B) expanded Quartzel fibers (20% RH, 9 mW cm^{-2}).

was calculated around 2.7×10^{-3} and 1.3×10^{-2}, while the quantum efficiency for CO_2 production was 1.8×10^{-2} and 8.2×10^{-2} for the TiO_2 microfibers and for Quartzel®, respectively (Table 2). This meant that Φ_{CO_2} was 6.8 and 6.2 the quantum efficiency of heptane degradation $\Phi_{heptane}$ for each media, respectively, confirming an almost complete heptane mineralization in both cases. The results obtained with acetone and heptane thus lead to the higher efficiency of the Quartzel® fibers than the pure TiO_2 microfibers at 20% RH.

However, the degradation of toluene was found to be much slower on Quartzel® than on the TiO_2 microfibers. A clear change of the degradation rate was observed with both media: after a fast decrease of toluene degradation during the first 50–100 min, the rate slowed down to a higher extent with the commercial fibers. A prior study [47] of the photocatalytic oxidation of toluene observed catalyst deactivation for high toluene levels (>200 mg m^{-3} or 50 ppmV). Relative to heptane (also 7 carbon atoms), almost no CO_2 was produced from toluene with the Quartzel® fibers after 70 min (0.139 ppmV min^{-1} *i.e.* the same rate as the CO_2 entrance from outside atmosphere), while the rate of CO_2 formation with the pure TiO_2 microfibers was still 0.462 ppmV min^{-1} (twice less than with heptane). With the TiO_2 microfibers, $\Phi_{toluene}$ in the second step of the reaction is 2.4×10^{-3} (slightly smaller than that of heptane) while Φ_{CO_2} is 4 times higher, meaning a less complete mineralization than that of heptane. With the Quartzel fibers, the corresponding second-step quantum efficiencies were much lower (1.1×10^{-3} and 2.8×10^{-3} indicating a lower mineralization, Table 2). The picture of the Quartzel® fibers after toluene degradation (only 50% achieved after 1200 min irradiation) showed a yellowed media displaying some darkened lumps accounting for its loss of activity (Fig. 9). The media recovered its initial color, form and activity only after extensive (48 h) irradiation in the reactor with clean air at 20% RH. During this step, GC analysis could not detect any volatile by-product, probably due to their very slow release during this reconditioning step. On the other hand, the pure TiO_2 fibers remained uncolored and were able to degrade all the toluene within 1500 min, without sign of deactivation (continuous CO_2 increase).

Figure 9. Expanded Quartzel® inside the reactor after irradiation in the presence of toluene for 500 min.

4. Discussion

The aim of this study was to confirm the efficiency of lab-extruded pure TiO_2 microfibers for VOCs mineralization in a suitable recirculating flow-through reactor where the fibers could be laid out as a soft mat. Their efficiency was compared to that of a commercial photocatalytic media Quartzel®, made of TiO_2 coated quartz fibers, under strictly identical conditions, especially regarding light transmission by the two media. Under our experimental conditions, VOC adsorption on the media in the dark could not actually be determined and irradiation began after 10 min of flux equilibration in the dark.

One of the main results of these experiments is that lab-made-TiO_2 fibers were efficient for gas-phase mineralization of acetone, heptane and toluene and that they could be used repeatedly without any loss of activity, only flushing the reactor with fresh humid air after each irradiation.

For both fiber types, the kinetics was essentially zero order in acetone, consistent with the claim that the surface was nearly fully covered by acetone. CO_2 evolution was observed with both types of fibers, accounting for an almost complete acetone mineralization. With our fibers, the rate of CO_2 evolution was shown to be independent of initial acetone concentration, consistent with our claim of complete surface coverage for the acetone range of 50–500 ppmV used here. With both fibers, the rate of acetone degradation r_A or the quantum efficiency of acetone degradation $\Phi_{acetone}$ and the rate

of CO_2 formation r_{CO2} or the quantum efficiency of CO_2 production Φ_{CO_2} were maximum at 20% RH and then decreased for higher RH, in agreement with previous results [48,49,45]. At 20% RH, both r_A, $\Phi_{acetone}$, r_{CO2} and Φ_{CO_2} were 3–4 times higher with Quartzel® than with lab-made TiO_2 fibers, while at 60% RH the rates and quantum efficiencies were equal, reflecting the lower water sensitivity of our microfibers *vs.* Quartzel.

Last, the reaction rates should vary with the light intensity I as I^{α} with $\alpha = 1$ at low intensities and $\alpha = 0.5$ at high values [42]. With both types of fibers, we obtained a satisfactory linear correlation of r_A or r_{CO_2} with I (Figs. 6 and 7B), implying that $\alpha = 1$. This result means that the reaction behaves in both cases in the low irradiance regime from 2 to 9 mW cm^{-2}.

The reaction rate and quantum efficiency of heptane degradation, and the initial rate and quantum efficiency of CO_2 formation were once again 4–5 times higher with the Quartzel® fibers than with the lab-made TiO_2 fibers. With heptane however almost 100% mineralization yields were observed in both cases assuming that each molecule of heptane should give 7 molecules of CO_2. The much lower reaction rates, quantum efficiencies and poor mineralization yield obtained with the Quartzel® fibers for toluene degradation, together with their strong yellow color after irradiation was striking and implied a very fast poisoning of these fibers by the adsorbed reaction by-products usually observed (benzaldehyde, benzoic acid, and several aliphatic aldehydes and carboxylic acids) [47,50–52]. From the CO_2 formation curve of the lab-made TiO_2 fibers, which showed a continuous linear increase, it could be concluded that the mineralization of toluene could be completely achieved after extensive irradiation since after 1500 min the CO_2 level corresponded to half of the stoichiometric expectation.

To summarize, it may be concluded from our results that the behavior of both types of fibers for VOCs and water adsorption was completely different, in spite of a similar specific surface area in both cases: 110 $m^2 g^{-1}$ against 120 $m^2 g^{-1}$. This conclusion was also achieved when comparing the toluene or ethylene removal efficiency obtained on different TiO_2-based catalysts [53,54]. The Quartzel fibers were very sensitive to acetone adsorption since a Langmuir–Hinshelwood mechanism was satisfactorily modeled. They were also more sensitive to competitive water adsorption when increasing % RH in agreement with a recent study [33]. The TiO_2 microfibers were more efficient for the degradation of adsorbed high molecular weight aldehydes and carboxylic acids in the case of toluene. In other words, the pure TiO_2 lab-extruded fibers appear to be less sensitive to water, aldehydes and other by-products adsorption during the photocatalytic process, improving their efficiency relative to the commercial fibers under more severe conditions. These differences can tentatively be accounted for by the composition of the fibers (pure TiO_2 *vs.* Quartz coated TiO_2, anatase phase with small amount of brookite for the pure TiO_2 fibers) and by their structural parameters (fibers diameter and roughness, micro/mesoporosity, point of zero charge), even if to the best of our knowledge, some of these data are not available for Quartzel® fibers. The synergetic effects of several factors such as crystal phase, crystallinity, surface area-to-volume ratio and photon conversion efficiency of mesoporous titania microspheres was previously shown to influence the photocatalytic performance for toluene degradation [55]. It can be tentatively assumed that the mesoporous TiO_2 fibers, with a characteristic mesoscale roughness promote a confinement effect of toluene and of its adsorbed by-products inside the nanometric channels of the mesostructure, favoring their mineralization [53]. This effect would no longer hold in the case Quarztel® fibers made of deposited TiO_2 particles, which are very quickly deactivated by the adsorbed intermediate carboxylic acids and aldehydes. In the case of acetone and heptane, probably less adsorbed intermediates are formed and this confinement effect is no longer worth: reaction rates are governed by complex competitive adsorption effects of VOCs and water at this intermediate relative humidity (20% RH) [33]. Further studies, out of the scope of the present work, with heptane and toluene at various concentrations and different relative humidity would be necessary to address these issues.

5. Conclusion

This work was carried out to compare, under strictly identical conditions, the kinetics of VOCs mineralization of lab-extruded pure TiO_2 fibers prepared under easily scalable conditions with those of a commercial photocatalytic media from Saint-Gobain Quartzel®. A flow-through recirculating reactor loop with variable LEDs irradiation at 365 nm was specially designed. With such a setup, the mass transfer and the light flux were optimized.

Both types of fibers were very efficient for acetone and heptane degradation with high mineralization yields. At 20% RH, the reaction rate constants were higher with the commercial media, whereas at 60% the catalysts displayed equal activity for acetone conversion. Toluene mineralization was much faster on these lab-made fibers than on Quarztel®, which was more sensitive to poisoning by reaction by-products. These results evidence a clear difference in the VOCs, water and polar by-products adsorption between these two kinds of fibers.

All the experiments were carried out in a continuous recycle mode. These newly developed fibers can be produced at an industrial scale with a proven efficiency for VOCs degradation and mineralization. Since they are less sensitive to humidity than the commercial fibers, they could be most useful under actual ambient air conditions at higher RH (between 60 and 80 %). Moreover, even if they are brittle, these fibers do not loose TiO_2 particles as experienced with Quartzel® fibers. These fibers thus present a good alternative to other commercially available photocatalytic media for gas phase purification. They could possibly be woven for diversifying their applications.

Appendix A. Supplementary data

Supplementary data associated with this article can be found, in the online version, at http://dx.doi.org/10.1016/j.apcatb.2015.05.015

References

[1] S. Laufs, G. Burgeth, W. Duttlinger, R. Kurtenbach, M. Maban, C. Thomas, P. Wiesen, J. Kleffmann, Atmos. Environ. 44 (2010) 2341–2349.
[2] Y. Paz, Appl. Catal. B Environ. 99 (2010) 448–460.
[3] B. Sánchez, M. Sánchez-Muñoz, M. Muñoz-Vicente, G. Cobas, R. Portela, S. Suárez, A.E. González, N. Rodríguez, R. Amils, Chemosphere. 87 (2012) 625–630.
[4] W.-K. Jo, K.-H. Park, Chemosphere. 57 (2004) 555–565.
[5] A.H. Aïssa, E. Puzenat, A. Plassais, J.-M. Herrmann, C. Haehnel, C. Guillard, Appl. Catal. B Environ. 107 (2011) 1–8.
[6] C. Aprile, A. Corma, H. Garcia, Phys. Chem. Chem. Phys. 10 (2008) 769–783.
[7] W. Li, Z. Wu, J. Wang, A.A. Elzatahry, D. Zhao, Chem. Mater. 26 (2014) 287–298.
[8] R. Liu, Y. Ren, Y. Shi, F. Zhang, L. Zhang, B. Tu, D. Zhao, Chem. Mater. 20 (2008) 1140–1146.
[9] P. Innocenzi, L. Malfatti, Chem. Soc. Rev. 42 (2013) 4198–4216.
[10] D.G. Shchukin, D.V. Sviridov, J. Photochem. Photobiol. C-Photochem. Rev. 7 (2006) 23–39.
[11] S. Madhugiri, B. Sun, P.G. Smirniotis, J.P. Ferraris, K.J. Balkus Jr., Micropor. Mesopor. Mater. 69 (2004) 77–83.
[12] W. Nuansing, S. Ninmuang, W. Jarernboon, S. Maensiri, S. Seraphin, Mater. Sci. Eng. B. 131 (2006) 147–155.
[13] R.A. Caruso, J.H. Schattka, A. Greiner, Adv. Mater. 13 (2001) 1577–1579.
[14] Y. Lei, L.D. Zhang, G.W. Meng, G.H. Li, X.Y. Zhang, C.H. Liang, et al., Appl. Phys. Lett. 78 (2001) 1125–1127.
[15] B. Xiang, Y. Zhang, Z. Wang, X.H. Luo, Y.W. Zhu, H.Z. Zhang, D.P. Yu, J. Phys. Appl. Phys. 38 (2005) 1152.
[16] D. Li, Y. Xia, Nano Lett. 3 (2003) 555–560.
[17] B. Vigolo, A. Pénicaud, C. Coulon, C. Sauder, R. Pailler, C. Journet, P. Bernier, P. Poulin, Science 290 (2000) 1331–1334.

[18] N. Kinadjian, M.-F. Achard, B. Julián-López, M. Maugey, P. Poulin, E. Prouzet, R. Backov, Adv. Funct. Mater. 22 (2012) 3994–4003.
[19] L. Biette, F. Carn, M. Maugey, M.-F. Achard, J. Maquet, N. Steunou, J. Livage, H. Serier, R. Backov, Adv. Mater. 17 (2005) 2970–2974.
[20] H. Serier, M.-F. Achard, O. Babot, N. Steunou, J. Maquet, J. Livage, C.M. Leroy, R. Backov, Adv. Funct. Mater. 16 (2006) 1745–1753.
[21] J. Dexmer, C.M. Leroy, L. Binet, V. Heresanu, P. Launois, N. Steunou, C. Coulon, J. Maquet, N. Brun, J. Livage, R. Backov, Chem. Mater. 20 (2008) 5541–5549.
[22] C.M. Leroy, M.-F. Achard, O. Babot, N. Steunou, P. Massé, J. Livage, L. Binet, N. Brun, R. Backov, Chem. Mater. 19 (2007) 3988–3999.
[23] N. Brun, C.M. Leroy, J. Dexmer, H. Serier, F. Carn, L. Biette, R. Backov, Comptes Rendus Chim. 13 (2010) 154–166.
[24] N. Kinadjian, M. Le Bechec, T. Pigot, F. Dufour, O. Durupthy, A. Bentaleb, et al., Eur. J. Inorg. Chem. (2012) 5350–5359.
[25] N. Kinadjian, M. Le Bechec, C. Henrist, E. Prouzet, P. Poulin, W. Neri, E. Prouzet, S. Lacombe, R. Backov, Adv. Eng. Mater. 17 (2015) 36–44.
[26] N. Kinadjian, M. Le Bechec, C. Henrist, E. Prouzet, S. Lacombe, R. Backov, ACS Appl. Mater. Interfaces 6 (2014) 11211–11218.
[27] R. Backov, P. Poulin, W. Neri, N. Kinadjian, M. Le Bechec, S. Lacombe, Procédé de préparation de fibres macroscopiques de dioxyde de titane par extrusion unidirectionnelle continue, fibres obtenues et applications, application FR (2014), 1452984 03/04/2014.
[28] D. Avnir, M. Jaroniec, Langmuir 5 (1989) 1431–1433.
[29] E. Prouzet, C. Boissière, S.S. Kim, T.J. Pinnavaia, Micropor. Mesopor. Mater. 119 (2009) 9–17.
[30] L. Szatmáry, J. Šubrt, V. Kalousek, J. Mosinger, K. Lang, Catal. Today 230 (2014) 74–78.
[31] S. Kim, S.K. Lim, Appl. Catal. B Environ. 84 (2008) 16–20.
[32] H. Destaillats, M. Sleiman, D.P. Sullivan, C. Jacquiod, J. Sablayrolles, L. Molins, Appl. Catal. B Environ. 128 (2012) 159–170.
[33] A. Maudhuit, C. Raillard, V. Héquet, L. Le Coq, J. Sablayrolles, L. Molins, Chem. Eng. J. 170 (2011) 464–470.
[34] J.P. Rivière, P. Sargood, L. Molins, Media for Photocatalytic Filter, Saint-Gobain Quartz SAS (2010), US 2012/0063958 A1.
[35] D. Vione, C. Minero, V. Maurino, M.E. Carlotti, T. Picatonotto, E. Pelizzetti, Appl. Catal. B Environ. 58 (2005) 79–88.
[36] R.J. Brandi, M.A. Citroni, O.M. Alfano, A.E. Cassano, Chem. Eng. Sci. 58 (2003) 979–985.
[37] Q. Peng, B. Kalanyan, P.G. Hoertz, A. Miller, D.H. Kim, K. Hanson, L. Alibabaei, J. Liu, T.J. Meyer, G.N. Parsons, J.T. Glass, Nano Lett. 13 (2013) 1481–1488.
[38] M.J. Riley, B. Williams, G.Y. Condon, J. Borja, T.M. Lu, W.N. Gill, J.L. Plawsky, J. Appl Phys. 111 (2012) 74904, http://dx.doi.org/10.1063/1.3699370
[39] W. Choi, S.J. Hong, Y.-S. Chang, Y. Cho, Environ. Sci. Technol. 34 (2000) 4810–4815.
[40] J. Taranto, D. Frochot, P. Pichat, Ind. Eng. Chem. Res. 48 (2009) 6229–6236.
[41] G. Vincent, P.M. Marquaire, O. Zahraa, J. Photochem. Photobiol. Chem. 197 (2008) 177–189.
[42] J. Peral, D.F. Ollis, J. Catal. 136 (1992) 554–565.
[43] M.L. Sauer, D.F. Ollis, J. Catal. 149 (1994) 81–91.
[44] M. Bettoni, P. Candori, S. Falcinelli, F. Marmottini, S. Meniconi, C. Rol, G.V. Sebastiani, J. Photochem. Photobiol. Chem. 268 (2013) 1–6.
[45] A.V. Vorontsov, E.N. Kurkin, E.N. Savinov, J. Catal. 186 (1999) 318–324.
[46] A. Piscopo, D. Robert, C. Marzolin, J.V. Weber, J. Mater. Sci. Lett. 19 (2000) 683–684.
[47] Y. Luo, D.F. Ollis, J. Catal. 163 (1996) 1–11.
[48] S.B. Kim, Appl. Catal. B Environ. 35 (2002) 305–315.
[49] T.N. Obee, R.T. Brown, Environ. Sci. Technol. 29 (1995) 1223–1231.
[50] M.C. Blount, J.L. Falconer, Appl. Catal. B Environ. 39 (2002) 39–50.
[51] M. Lewandowski, D.F. Ollis, Appl. Catal. B Environ. 45 (2003) 223–238.
[52] J. Mo, Y. Zhang, Q. Xu, Y. Zhu, J.J. Lamson, R. Zhao, Appl. Catal. B Environ. 89 (2009) 570–576.
[53] F. Bosc, D. Edwards, N. Keller, V. Keller, A. Ayral, Thin Solid Films. 495 (2006) 272–279.
[54] X. Wang, J.C. Yu, C. Ho, Y. Hou, X. Fu, Langmuir. 21 (2005) 2552–2559.
[55] Y. Feng, L. Li, M. Ge, C. Guo, J. Wang, L. Liu, ACS Appl. Mater. Interfaces 2 (2010) 3134–3140.